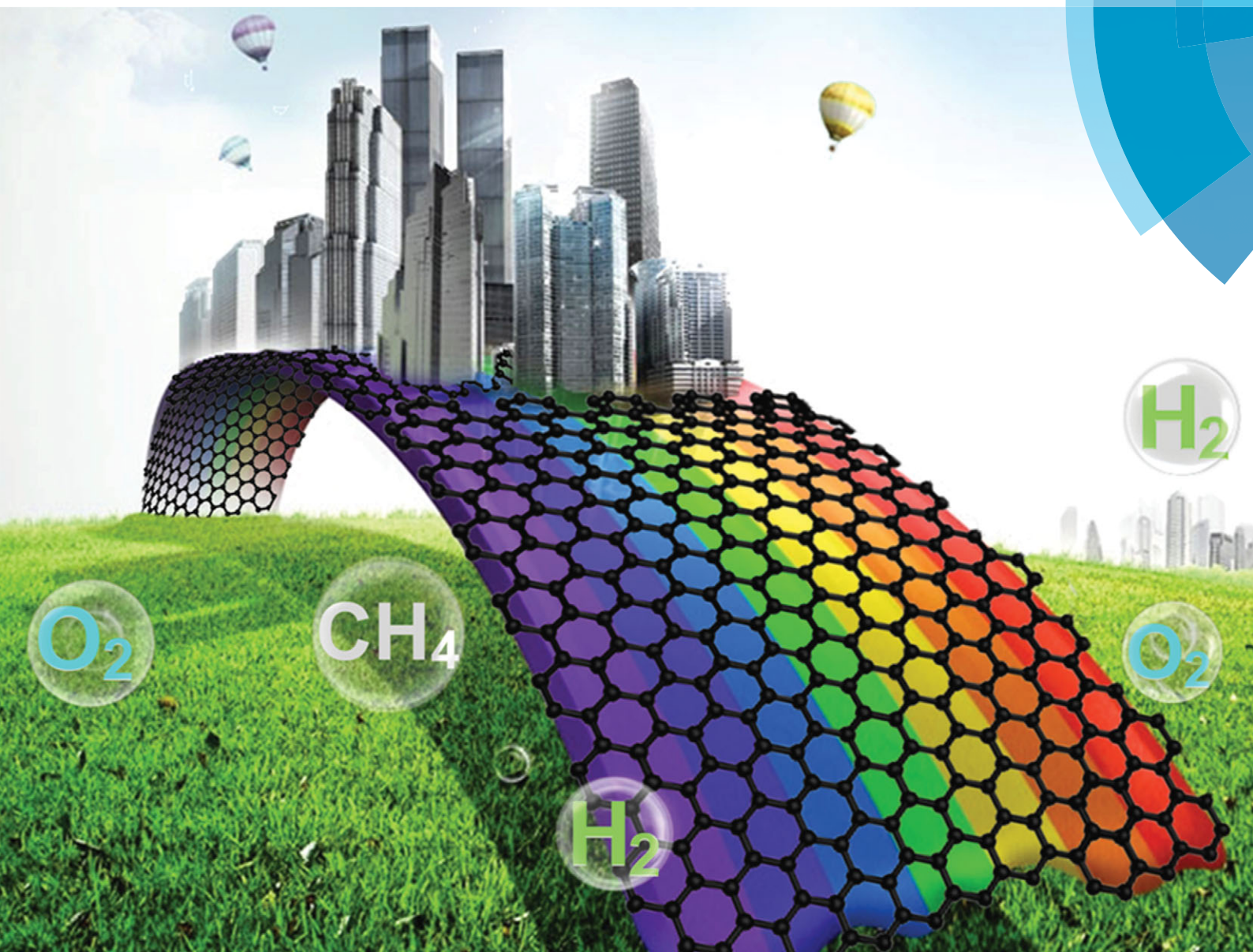


# Chem Soc Rev

Chemical Society Reviews

[www.rsc.org/chemsocrev](http://www.rsc.org/chemsocrev)



ISSN 0306-0012



REVIEW ARTICLE

Mario Pagliaro, Yi-Jun Xu *et al.*

Artificial photosynthesis over graphene–semiconductor composites. Are we getting better?



Cite this: *Chem. Soc. Rev.*, 2014, 43, 8240

# Artificial photosynthesis over graphene–semiconductor composites. Are we getting better?†

Min-Quan Yang,<sup>ab</sup> Nan Zhang,<sup>ab</sup> Mario Pagliaro<sup>\*c</sup> and Yi-Jun Xu<sup>\*ab</sup>

Tremendous interest is devoted to fabricating numerous graphene (GR)–semiconductor composites toward improved conversion of solar energy, resulting from the observation that the photogenerated electrons from semiconductors (e.g., TiO<sub>2</sub>, CdS) can be readily accepted or shuttled in the two-dimensional (2D) GR sheet. Yet although the hunt is on for GR–semiconductor composite based photoredox applications that aim to exploit the remarkable electronic conductivity of GR, the work necessary to find out how it could best be harnessed to improve the photocatalytic performance of semiconductors remains scanty. In this review, we highlight a few problems associated with improving the photocatalytic performance of semiconductors *via* methodological coupling with GR. In particular, we address strategies for harnessing the structure and electronic conductivity of GR *via* strengthening the interfacial contact, optimizing the electronic conductivity of GR, and spatially optimizing the interfacial charge carrier transfer efficiency. Additionally, we provide a brief overview of assembly methods for fabricating GR–semiconductor composites with controllable film infrastructure to meet the requirements of practical photocatalytic applications. Finally, we propose that, only with the principle of designing and understanding GR–semiconductor composites from a system-level consideration, we might get better at imparting the power of GR with unique and transformative properties into the composite system.

Received 24th June 2014

DOI: 10.1039/c4cs00213j

[www.rsc.org/csr](http://www.rsc.org/csr)

<sup>a</sup> State Key Laboratory of Photocatalysis on Energy and Environment, College of Chemistry, Fuzhou University, Fuzhou 350002, P. R. China

<sup>b</sup> College of Chemistry, New Campus, Fuzhou University, Fuzhou 350108, P. R. China. E-mail: yjxu@fzu.edu.cn

<sup>c</sup> Istituto per lo Studio dei Materiali Nanostrutturati, CNR, via U. La Malfa 153, 90146 Palermo, Italy. E-mail: mario.pagliaro@cnr.it

† Electronic supplementary information (ESI) available: Appendix of other additional references related to the various applications of GR-based composite photocatalysts, which are available for readers who want to access the literature for further reading. See DOI: 10.1039/c4cs00213j

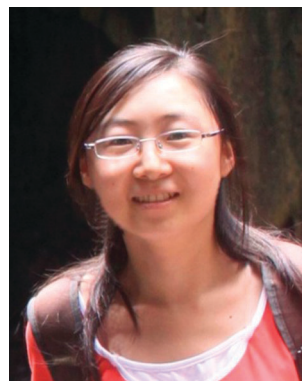
## 1. Introduction

With the ever-increasing global energy demand and environmental crisis, finding and using renewable and clean energy resources has become one of the most important and challenging tasks for human society.<sup>1–3</sup> Artificial photosynthesis, a well-orchestrated mimic of natural photosynthesis observed in green plants and a few other micro-organisms,<sup>4–6</sup> allows the direct conversion of sunlight into chemical energy, thus providing an opportunity to



Min-Quan Yang

*Min-Quan Yang is a chemistry scholar based at State Key Laboratory of Photocatalysis on Energy and Environment at Fuzhou, P. R. China. His main research interests focus on the synthesis of carbon-based materials, especially graphene-based composite nanomaterials for applications in heterogeneous photocatalysis.*



Nan Zhang

*Nan Zhang is a chemistry scholar based at State Key Laboratory of Photocatalysis on Energy and Environment at Fuzhou, P. R. China. Her main research interests include the fabrication of core-shell and carbon-based nanocomposites for potential target applications in heterogeneous photocatalysis.*

address the environmental and energy issues.<sup>5–8</sup> The original demonstration of artificial photosynthesis can date back to the discovery of water splitting achieved under UV radiation with TiO<sub>2</sub>.<sup>9</sup> Since then, many different photocatalyst materials, such as semiconductors, transition-metal complexes, and so on, have been developed and extensively studied for diverse artificial photosynthesis processes.<sup>4,10–12</sup>

In recent years, ignited by the advent of graphene (GR),<sup>13</sup> which displays exceptional mechanical, thermal, optical, and electrical properties and unique two-dimensional (2D) morphology,<sup>14,15</sup> there has been significantly increasing research interest in utilizing GR to construct novel GR-based semiconductor composite photocatalysts.<sup>16–18</sup> The excellent electron conductivity, unique 2D morphology and high transparency of GR make it an ideal platform to assemble semiconductor components and accept/transport photogenerated charge carriers, thereby improving the efficiency of the photocatalytic processes.<sup>19–21</sup> To date, various GR–semiconductor composite based artificial photosynthesis systems with enhanced photocatalytic performance have been designed and widely applied in a myriad of fields, including environmental remediation,<sup>22,23</sup> water splitting,<sup>24,25</sup> CO<sub>2</sub> photoreduction,<sup>26–28</sup> and selective organic transformation.<sup>18,29,30</sup>

For the synthesis of GR–semiconductor composite photocatalysts, graphene oxide (GO) is often used as the precursor of GR.<sup>15,17,18,31</sup> The versatile multi-faces of GO in a solution phase, such as acting as a 2D random diblock polymer, highly anisotropic colloid or amphiphile, make it an unconventional 2D soft material apart from making GR.<sup>32–35</sup> Additionally, the abundant oxygenated functional groups (*e.g.*, –OH, –COOH, epoxide together with structural defects) on the GO surface provide anchoring points for introducing selective functionality.<sup>36–39</sup> These prominent features impart GO with the ample solution processability and unique structure-directing role in inducing the solution-phase nucleation and growth of other components on its surface, *e.g.*, the assembly of semiconductor (TiO<sub>2</sub>, CdS, ZnO, *etc.*) ingredients on GO.<sup>20,40–42</sup> Following the chemical, thermal or photo-treatments, GO can be readily reduced to GR,<sup>43–45</sup> often referred to as reduced GO (RGO). As a result, a variety of GR (or RGO)–semiconductor composites have been reported for the potential applications in photocatalysis.

Thus far, coupling semiconductors with GR is widely recognized to be a viable strategy to improve the photocatalytic performance of semiconductors because GR is an electronically conductive 2D platform enabling the acceptance and shuttle of photogenerated electrons from band-gap-excitation of semiconductors.<sup>15,24,46</sup> Consequently, the boosted lifetime and transfer of charge carriers in the GR–semiconductor systems contribute to improving the photocatalytic activity of semiconductors.<sup>15,16,22</sup> Nevertheless, despite the massive reports on GR–semiconductor photocatalysts,<sup>21,22,24</sup> we still lack a good understanding of how to sufficiently take advantage of the unique properties and great potential of GR, such as the excellent electron conductivity. In particular, the significant, in-depth fundamental studies on understanding how to maximize the charge carrier separation and transfer efficiency across the interfacial domain of GR–semiconductor composites have received little attention.

This review will predominantly highlight a few problems that need to be addressed regarding GR–semiconductor composite photocatalysts, which are based on the progress made by our group and examination of typical key advances in the literature. First, we show that it would be irrational to ascribe the photocatalytic activity enhancement to the ideal excellent electron conductivity of GR for GR–semiconductor composites that are prepared by the random integration approach. Second, we demonstrate the strategies to harness the structure and electronic conductivity of GR *via* strengthening the interfacial contact and optimizing interface composition. In particular, the photocatalytic activity enhancement of GR–semiconductor composites is not just an issue of interfacial contact, but it is also the optimization of interfacial composition that spatially influences the microscopic charge carrier transfer pathways. Then, from a viewpoint of practical applications, we describe a brief overview of assembly methods for fabricating GR–semiconductor composite photocatalysts with controllable film infrastructure. Finally, we cast a personal prospect on the future progress on how to further boost the photocatalytic performance of GR–semiconductor composite materials toward more efficient solar energy conversion. We hope that this review could help realize the key fundamental issues in this research field that have not been well addressed yet



**Mario Pagliaro**

*Mario Pagliaro is a research chemist based at Italy's Research Council in Palermo. His research and educational interests encompass a broad field from sol-gel functional materials to helionomics, a term he introduced in 2008. Mario has been chairing the SuNEC and FineCat international meetings held annually in Sicily since 2011.*



**Yi-Jun Xu**

*Yi-Jun Xu is a full professor now working at State Key Laboratory of Photocatalysis on Energy and Environment at Fuzhou, P. R. China. His current research interests primarily focus on the assembly and applications of semiconductor-based nano-structured materials, such as graphene-based and core-shell composite photocatalysts, in the field of heterogeneous photocatalysis.*

in the literature, which in turn facilitates the rational processing and property control of GR–semiconductor composite photocatalysts toward targeting artificial photoredox applications.

## 2. To be rational about a long story

An overview of the literature on GR–semiconductor composites reveals that the photoactivity enhancement is attributed to the excellent or superior electron conductivity of GR, which results in the enhanced separation of electron–hole pairs photogenerated from semiconductors (Fig. 1).<sup>15,17,24</sup> However, recalling the original concept of GR can remind us that the fact is not the case. GR is the name given to an individual sheet of  $sp^2$ -hybridized carbon atoms bound in two dimensions.<sup>13,47,48</sup> The excellent electronic, optical and physicochemical properties of GR are intrinsically associated with an ideal single-layer and defect-free 2D sheet,<sup>47–50</sup> which has been hardly realized in the reported GR–semiconductor composites because of the following fundamental reasons.

Regarding the preparation of GR–semiconductor composite photocatalysts, the most common approach is using GO,<sup>15,18,24</sup> synthesized from modified Hummers' method,<sup>51</sup> as the precursor of GR. The plentiful oxygenated functional groups on the GO sheet enable it to disperse well in water and many other polar solvents, providing an accessible platform to construct GR–semiconductor composites.<sup>18,52–54</sup> However, the oxygenated functionalization of GO results in considerable disruption of the electronic structure of GR; the abundant oxygen moieties inevitably break the 2D  $\pi$ -conjugation of original GR sheets.<sup>34,36,55,56</sup> Although these oxygenated groups can be removed by reduction, large defect populations still remain, as illustrated in Fig. 2.<sup>36,56</sup> The electronic conductivity of GR (RGO) derived from the GO

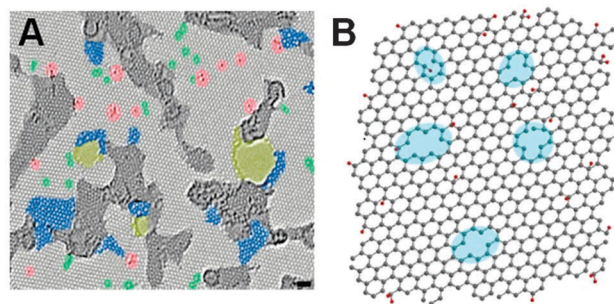


Fig. 2 (A) Colour scheme highlighting the different structural features of RGO: light-gray, defect free crystalline graphene area; dark grey, contaminated regions; blue, disordered single-layer carbon networks or extended topological defects; red, individual adatoms or substitutions; green, isolated topological defects; and yellow, holes and their edge reconstructions. Scale bar: 1 nm. Reprinted with permission from ref. 56. Copyright 2010 American Chemical Society. (B) Atomic model schematically illustrating the RGO basal plane consisting of holes, topological defects and remnants of oxygen groups.

precursor is actually lower than ideal single-layer and defect-free GR sheets.<sup>13,36,55</sup> Thus, strictly speaking, GO-derived graphene should be named reduced GO (RGO). However, this definition is not unambiguously unified in the literature.<sup>15,24,57,58</sup> Conversely, once the enhanced photoactivity of RGO–semiconductor composites is obtained, researchers are inclined to attribute this photoactivity enhancement to the excellent electronic conductivity of graphene (GR) while not mentioning the significant difference of electronic conductivity between GO-derived GR and single-layer, defect free GR.

On the other hand, during the wet chemistry synthesis of GR–semiconductor composites, GO-derived GR (RGO) often suffers from irreversible aggregation, being present in the multi-layer form or restacking into a graphitic structure.<sup>15,59–61</sup> The aggregation of GR results in a striking change in its properties, which particularly would further weaken the electrical conductivity and lower the surface area and optical transparency of GR.<sup>13,15,47,49</sup> Thus, under such circumstances, whether GR actually displays the “unique, excellent electronic conductivity” accounting for the photoactivity improvement of semiconductors deserves careful attention.

In 2010, Xu *et al.* argued that  $TiO_2$ –GR composite photocatalysts, obtained *via* a random “hard” integration of solid  $TiO_2$  nanoparticles and GO followed by reduction of GO to GR, are in essence the same as other  $TiO_2$ –carbon (carbon nanotubes, fullerenes, and activated carbon) counterparts with regard to enhancing the photoactivity of  $TiO_2$ .<sup>14</sup> The key features for the prepared  $TiO_2$ –GR nanocomposites, including the increased adsorptivity of pollutants, enhanced light absorption intensity and extended light absorption range, promoted charge separation and transportation, and decreased photocatalytic activity with high content of GR, can also be observed in their counterparts of  $TiO_2$ –CNT prepared *via* the same approach. This work was reported since that GR has triggered a “gold rush” for exploiting its potential applications in both experimental and theoretical areas. It reminds researchers to rationally evaluate the role of GR in the as-fabricated GR-based nanocomposites

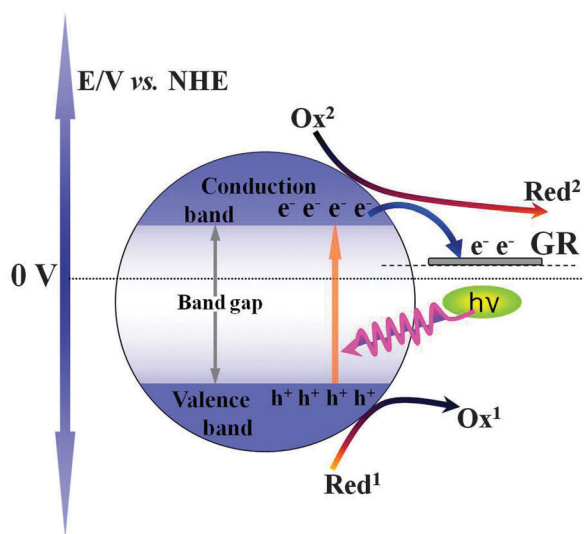


Fig. 1 A simplified schematic description of the photocatalytic process over the composites of the GR–semiconductor (e.g.,  $TiO_2$ , CdS, and ZnO) where due to the energy level match, GR is able to accept, store and shuttle photogenerated electrons from semiconductors, thereby promoting the separation and transfer of charge carriers (electron–hole pairs) for improved artificial photoredox reactions.

instead of separately emphasizing the unique and outstanding properties of GR.<sup>14</sup>

Indeed, this issue was pertinently discussed by the editorials in *Nature* in 2011,<sup>62</sup> which was based on a meeting on “Graphene: The Road to Applications”. Though GR has remarkable properties, we are still not fully clear about how these intriguing characteristics can be best harnessed, and this situation is more prominent in the field of GR–semiconductor composite based artificial photocatalysis.<sup>62</sup> The random integration of GR with semiconductors cannot manifest the unique and prominent advantages of GR over its forebears (*e.g.*, carbon nanotubes) in enhancing the semiconductor photoactivity.<sup>14</sup> It would not be objective to attribute the photoactivity improvement to a little vague but “panacea” words of the unique, excellent electronic conductivity of graphene (GR), a name widely and loosely used in the literature.<sup>15–18</sup> The electronic conductivity and mobility of GR changes dramatically when it interacts with the surrounding environment or its structure and morphology are changed. GR, even in the ideal state, is just a very promising material, not a miracle one.<sup>62</sup> It is crucial to identify and acknowledge many practical hurdles for fabricating the GR-based devices.

But this should not necessarily be discouraging. Looking back at the history of materials science, for any new materials, it typically takes 20 years or more to emerge from the lab and be commercialized.<sup>63</sup> In this sense, the construction of the next-generation of photocatalytic systems based on GR–semiconductor composites, which potentially are able to integrate conversion, storage of solar energy and accomplishing multistep photocatalytic processes, would take a much longer time than people think and we should be more rational about this long story.

### 3. How to maximize the interfacial charge carrier transfer efficiency

As the proverb goes, every coin has two sides. For the preparation of graphene–semiconductor composite photocatalysts, the GO-derived graphene (*aka* RGO) is more defective and less conductive; however, owing to the low cost, facile preparation and flexible solution processability of GO, RGO is able to be made in bulk and is widely used in many architecture forms catering to the need of potential applications.<sup>15–22</sup> In contrast, the high-quality, unoxidized GR, as generally prepared by micromechanical cleavage or chemical vapor growth, has few or no defects, but this type of GR cannot be made in large quantity and particularly the relatively low solution processability hampers its wide use in the wet chemistry synthesis of GR–semiconductor composite photocatalysts.<sup>15,18</sup> Therefore, to achieve efficient GR–semiconductor composite photocatalysts independent of which type of GR is adopted, we should best bring the advantageous property side of GR into full play and simultaneously alleviate its intrinsic disadvantages, thereby maximizing the net efficiency of improving the photoactivity of GR–semiconductor composites rather than imposing “panacea” praise on the unique and superior excellent electronic conductivity

of GR. To this end, tremendous effort has been devoted to exploring multifarious strategies to harness the structure and electronic conductivity of GR by maximizing the interfacial charge carrier transfer efficiency, which has proven to be effective to enhance the semiconductor photoactivity.

#### 3.1 Strategy to optimize the electronic conductivity of graphene

**3.1.1. Decreasing the defects of graphene.** To use defect-free and aggregation-resistant graphene would be a straightforward strategy to exploit the outstanding electronic properties of graphene. Inspired by the solvent dispersion of carbon nanotubes, Coleman *et al.* have reported the noncovalent solution-phase methods to give defect-free or defect-few graphene by exfoliating graphite powder in a suitable solvent with appropriate surface energy matching that of graphene,<sup>64–67</sup> which is referred to as solvent-exfoliated graphene (SEG).

Decreasing the defect density of graphene has been evidenced to contribute to improving the photoactivity of semiconductors by recent research works.<sup>68,69</sup> For instance, Hersam *et al.* have reported the utilization of SEG to prepare SEG–TiO<sub>2</sub> nanocomposites, which display enhanced photocatalytic activity.<sup>68</sup> In this work, the SEG was produced *via* ultrasonic treatment of natural graphite in *N,N*-dimethylformamide (DMF). Fig. 3B displays the typical Raman spectroscopy of the resulting SEG and the solvent-reduced graphene oxide (SRGO) obtained from the reduction of GO, from which it can be calculated that the intensity ratio of the D and G bands ( $I_D/I_G$ ) for SEG is 0.17, which is much lower than 0.82 for SRGO.<sup>68</sup> Due to the  $I_D/I_G$  being a measure of the relative concentration of local defects or disorders (particularly the sp<sup>3</sup> hybridized defects) compared to the sp<sup>2</sup> hybridized graphene domains,<sup>68,69</sup> the lower  $I_D/I_G$  value of SEG indicates that it has a much lower defects density. Fig. 3A shows that the sheet resistance of SRGO films was on average 2.4 times higher than SEG films at the same areal mass density, which is consistent with its higher defect density. The results indicate that the defect has a significant influence on the electrical conductivity<sup>55</sup> and would change the properties of graphene.<sup>70</sup> The photocatalytic activity of the SEG–TiO<sub>2</sub> and SRGO–TiO<sub>2</sub> nanocomposites at various compositions has been evaluated *via* acetaldehyde (CH<sub>3</sub>CHO) photooxidation and CO<sub>2</sub> photoreduction reactions. As shown in Fig. 3C, the photoactivities achieved over the optimal SEG–TiO<sub>2</sub> nanocomposites are *ca.* 3.0 times and 2.3 times as high as those of the optimum SRGO–TiO<sub>2</sub> counterparts under visible light irradiation in terms of the oxidation rate and the produced rate of methane, respectively.

In another work, Xu *et al.* fabricated a series of graphene (SEG and RGO)–TiO<sub>2</sub> nanocomposites following a facile “soft” chemistry approach using SEG and GO as the precursors of graphene, respectively.<sup>69</sup> Toward selective oxidation of different benzylic alcohols and allylic alcohols under visible light irradiation, the as-synthesized SEG–TiO<sub>2</sub> nanocomposites also display higher photoactivities than their counterparts of RGO–TiO<sub>2</sub>, as shown in Fig. 3D. This is mainly because the SEG sheet with lower defect density and sheet resistance has superior

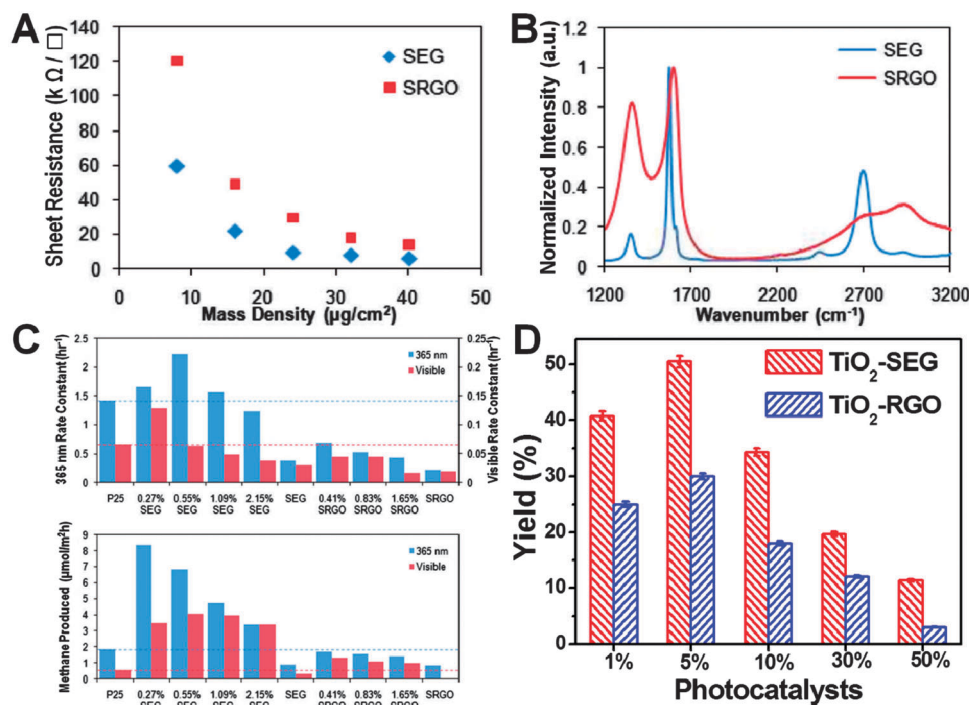


**Fig. 3** (A) Sheet resistance of SEG and solvent-reduced graphene oxide (SRGO) thin films formed *via* vacuum filtration as a function of mass density; (B) intensity-normalized Raman spectra of SEG and SRGO films annealed at 400 °C for 30 min in air; and (C) photocatalytic activity of SEG–P25 and SRGO–P25 nanocomposites toward (top panel) pseudo-first-order CH<sub>3</sub>CHO photo-oxidation and (bottom panel) CO<sub>2</sub> photoreduction under ultraviolet (365 nm) and visible illumination. Reprinted with permission from ref. 68. Copyright 2011 American Chemical Society. (D) Photocatalytic selective oxidation of benzyl alcohol to benzaldehyde over the TiO<sub>2</sub>–SEG and TiO<sub>2</sub>–RGO nanocomposites under visible light irradiation for 4 h at room temperature (the values of x-axis are short for the weight addition ratios of GR). Reprinted with permission from ref. 69. Copyright 2012 Royal Society of Chemistry.

electronic coupling to semiconductors, which allows photo-excited energetic electrons to diffuse farther from the graphene–semiconductor interface, facilitates the separation and transfer of photogenerated charge carriers, and thus enhances the photocatalytic performance.<sup>68,69</sup> These research studies faithfully demonstrate that the use of SEG with a lower defect density as the precursor of graphene can further improve the photo-activity of graphene–semiconductor nanocomposites. However, the low solution processability and difficulty of production in large quantities with high quality significantly limit the research interest in the use of SEG for constructing GR–semiconductor composites for photocatalytic applications.

### 3.1.2. Constructing graphene-based 3D macrostructures.

Despite the relatively high defect density of RGO, considerable interest has been paid to utilize GO as the precursor of GR to fabricate a myriad of RGO–semiconductor composite photocatalysts because of the easy, flexible processability and structure-directing role of GO in a solution phase.<sup>71–73</sup> The physiochemical and electronic properties of RGO can be readily tuned by architectural engineering of the structure and morphology of RGO.<sup>74–78</sup> Numerous methods, including self-assembly,<sup>79–81</sup> template guided growth,<sup>76,82–85</sup> solvothermal reaction,<sup>41,71,86,87</sup> organic sol–gel reaction<sup>88–90</sup> and LightScribe patterning technology,<sup>91,92</sup> have been developed to transform the 2D RGO sheets into 3D macroscopic structures (*e.g.*, porous films, foams, aerogels, scaffolds and networks). For more details, please refer to the recent review articles, which have summarized

and discussed these methods in detail.<sup>93,94</sup> The construction of 3D graphene affords a feasible approach to ameliorate the structural and electronic properties of graphene, by which the photocatalytic performance of RGO–semiconductor composites is optimized. Additionally, the 3D architectures impart other favorable properties, such as a large accessible surface area, aggregation resistance, interconnected conductive frameworks, fast mass kinetics and a special microenvironment.<sup>41,93,94</sup> Notably, the overall photocatalytic performance of graphene–semiconductor composites is not the only issue of the electronic conductivity contribution of graphene to improving the charge carrier separation and transfer. Other factors, *e.g.*, the surface area, mass transfer kinetics and local ensemble environment, could have a synergistic influence on the photocatalytic redox processes. Therefore, the fine-tuning of 3D structural morphology of RGO represents a versatile strategy for the optimization of photoactivity of RGO–semiconductor composites for a given target reaction.

For example, Zhang *et al.* have recently reported the fabrication of 3D-structured TiO<sub>2</sub>/RGO aerogel (GA) nanocomposites *via* a simple one-step hydrothermal method,<sup>41</sup> which uses glucose as the linker and face-controlling agent to produce (001) facets and a mesoporous structure on TiO<sub>2</sub>, as illustrated in Fig. 4A and B. During the hydrothermal process, the hydroxyl groups at one end of glucose connect with GR while the hydroxyl groups at the other end connect with the TiO<sub>2</sub> facets, facilitating the *in situ* growth of ultradispersed TiO<sub>2</sub> nanocrystals on the GA surface

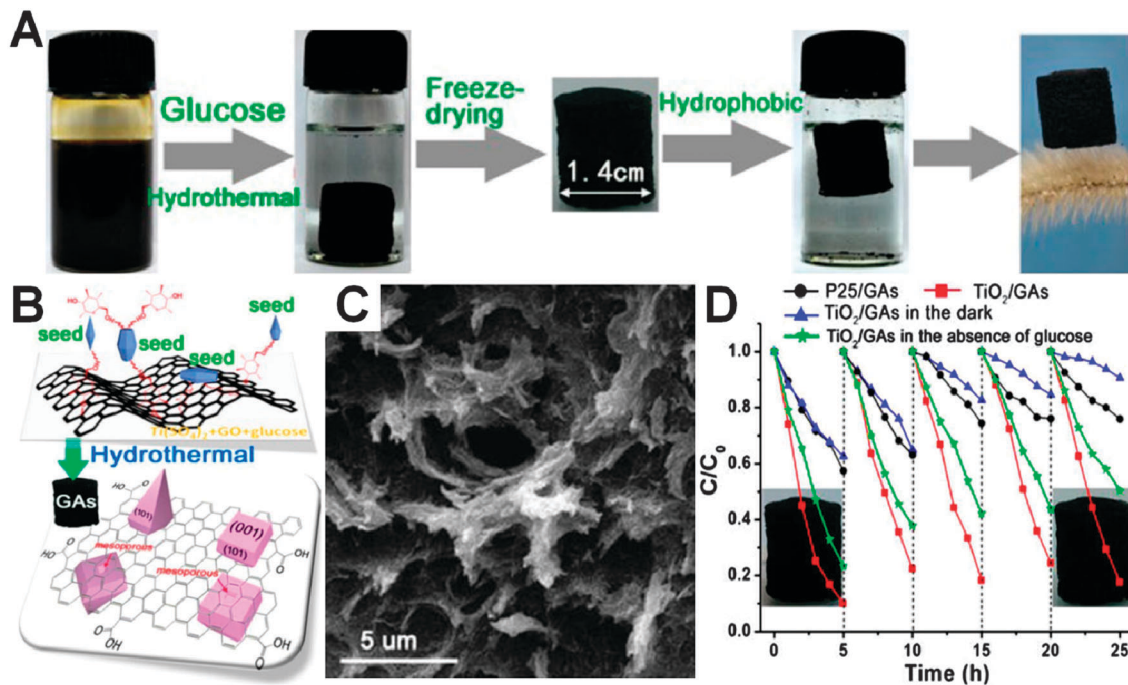


Fig. 4 (A) Appearance illustration of  $\text{TiO}_2$ -GAs involving glucose; (B) glucose-linked transformation pathway for the *in situ* growth of  $\text{TiO}_2$  nanocrystals with (001) facets on the GA surface; (C) SEM image of  $\text{TiO}_2$ -GAs (67 wt%) synthesized in the presence of glucose; and (D) cycling photodegradation of methyl orange (MO) under simulated solar light irradiation (with an AM 1.5 air mass filter). Reprinted with permission from ref. 41. Copyright 2014 American Chemical Society.

and affording strong interactions between  $\text{TiO}_2$  and GA. The resulting 3D  $\text{TiO}_2$ -GAs exhibit obvious hydrophobic properties and massive appearance (Fig. 4A), which is beneficial for the recycling of the catalyst for photocatalytic applications. Fig. 4C shows the typical SEM image of  $\text{TiO}_2$ -GAs. The  $\text{TiO}_2$ -GAs display a macroporous structure and the surface area of  $\text{TiO}_2$ -GAs can be up to  $204 \text{ m}^2 \text{ g}^{-1}$ . The hierarchical channels and high specific area are able to improve the adsorption of organic pollutants. In addition, the introduction of conductive GAs into the matrix of  $\text{TiO}_2$  enhances the electrical conductivity of  $\text{TiO}_2$ -GAs as compared to pure  $\text{TiO}_2$  and facilitates the electron transfer of the  $\text{TiO}_2$ -GA composite. Thus, the  $\text{TiO}_2$ -GAs display highly active and recyclable photocatalytic performance toward degradation of methyl orange pollutant (Fig. 4D), which can be ascribed to the synergetic effects of the strong interaction between  $\text{TiO}_2$  and GAs, facet characteristics, high electrical conductivity, large surface area, massive appearance and hydrophobic properties of the  $\text{TiO}_2$ -GA composites.

### 3.2 Strategy to strengthen the interfacial contact between graphene and semiconductors

**3.2.1. Utilizing the “structure-directing” role of GO for *in situ* growth of semiconductors.** Considering that the photo-generated charge carrier transfer predominantly occurs across the interfacial domain in GR-semiconductor composite systems, maximizing the interfacial contact between GR and the photo-active semiconductor is another strategy for harnessing the electronic conductivity of GR. The inherent oxygenated functionality endows GO with the unique structure directing role in

a solution phase, which allows for the even nucleation and growth of other components on the 2D sheet of GR, resulting in the controllable synthesis of GO-derived GR-semiconductor composites.<sup>15,18,26</sup>

In the case of using GO as the precursor of GR, two kinds of wet chemistry methods have been widely adopted to fabricate GR-semiconductor composite photocatalysts. One is the soft integration of GR with a soluble precursor of semiconductors instead of solid semiconductor particles. For this method, the “structure-directing” role of GO is used to induce the *in situ* anchoring of semiconductor particles in a solution phase.<sup>40,95,96</sup> The RGO-semiconductor composites obtained by this soft method often have good interfacial contact and a unique structure or morphology composition. For example, Sow *et al.* have reported that GO plays an essential role in the transition of the growth mechanism of  $\text{Cu}_2\text{O}$  from conventional ion-by-ion growth to non-classical particle-mediated crystallization under hydrothermal conditions, resulting in RGO-conjugated  $\text{Cu}_2\text{O}$  nanowire 3D mesocrystals.<sup>97</sup> Li *et al.* have reported the fabrication of CdS-cluster-decorated graphene nanosheets through a facile one-step *in situ* solvothermal strategy, during which the addition of GO changes the structure and morphology of the CdS semiconductor.<sup>98</sup> As shown in Fig. 5A and B, blank CdS shows a significant aggregation of small nanoparticles, and the diameters of the spherical CdS particles are around 100 nm. However, for the CdS-GR nanocomposite (GC), the much smaller CdS clusters are uniformly and tightly spread on the graphene with intimate interfacial interaction, forming a large layered structure. Fig. 5C displays the activities of photocatalytic

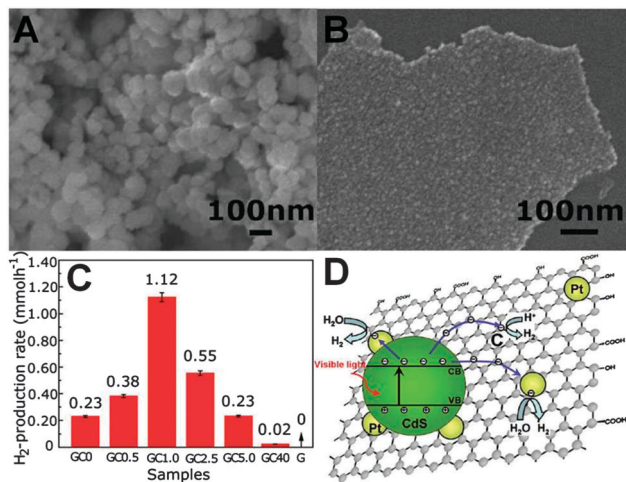


Fig. 5 SEM images of (A) blank CdS (GC0) and (B) CdS–1% GR (GC1.0); (C) comparison of the visible light photocatalytic activity of samples GC0, GC0.5, GC1.0, GC2.5, GC5.0, GC40, and G for H<sub>2</sub> production using 10 vol% lactic acid aqueous solution as a sacrificial reagent and 0.5 wt% Pt as a co-catalyst ( $\lambda > 420$  nm); and (D) schematic illustration of the charge separation and transfer in the graphene–CdS system under visible light irradiation. Reprinted with permission from ref. 98. Copyright 2011, American Chemical Society.

hydrogen production under visible light irradiation using Pt as a co-catalyst, which shows that the introduction of an appropriate amount of GR remarkably enhances the photoactivity of the CdS–GR nanocomposites. The higher photocatalytic activity of CdS–GR arises from the positive effect of GR, which serves as an electron collector and a source of active sites. The electrons photogenerated from the conduction band of semiconductor CdS not only transfer to the co-catalyst of Pt, but also to the carbon atoms on the graphene sheets, which are accessible to protons that could readily transform to H<sub>2</sub> (Fig. 5D).<sup>98</sup>

Additionally, by harnessing the unique and versatile structure-directing features of GO in a solution phase, Xu *et al.* have constructed RGO–TiO<sub>2</sub> composites with intimate interfacial contact, which exhibit significantly higher visible light photoactivity toward selective oxidation of alcohols than their counterpart with poor interfacial contact.<sup>59</sup> Further encouraging results are the simultaneous morphology control, defect engineering and photoactivity tuning of semiconductor ZnO by utilizing the surfactant properties of GO in a liquid phase.<sup>99</sup> By varying the amount of GO during the synthesis, the morphology of ZnO evolves from a one dimensional prismatic rod to a hexagonal tube-like architecture, as shown in Fig. 6A and B. The significant effect of GO on controlling the morphology of ZnO structures is aroused from the abundant functional groups (*e.g.*, –OH and –COOH) attached to its basal plane, which can favorably bind to the metal ions and change the kinetics of nucleation and growth of ZnO crystals, thus enabling GO to perform as a novel macromolecular surfactant. In addition, the ZnO crystals directly grown on the graphene sheets also lead to the intimate spatial interaction between the graphene network and ZnO (Fig. 6C). The good interfacial contact and unique structural composition are more advantageous for the separation and transfer of

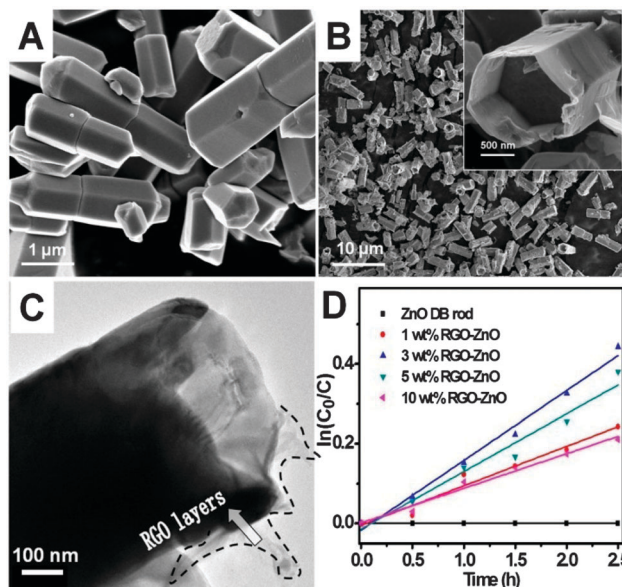


Fig. 6 SEM images of (A) a blank ZnO dumbbell-shaped (DB) rod and (B) 3 wt% RGO–ZnO (the inset is the SEM image at higher magnification); (C) TEM image of 3 wt% RGO–ZnO; and (D) photocatalytic reduction of Cr(VI) over the blank ZnO DB rod and RGO–ZnO nanocomposites under visible light irradiation ( $\lambda > 400$  nm). Reprinted with permission from ref. 99. Copyright 2014 Royal Society of Chemistry.

photogenerated charge carriers, leading to the photoactivity improvement more effectively, as displayed in Fig. 6D.

**3.2.2. Tuning the surface charge for self-assembly construction of graphene–semiconductor.** This method is based on the substantial electrostatic interaction between GO or GR and semiconductors with opposite surface charge, which is often used as a versatile bottom-up nanofabrication technique,<sup>100–105</sup> as exemplified in Fig. 7A.<sup>101</sup> The issue of strengthening interface contact can be assisted by the surface modification. The specific advantage of this approach over the above-mentioned method is

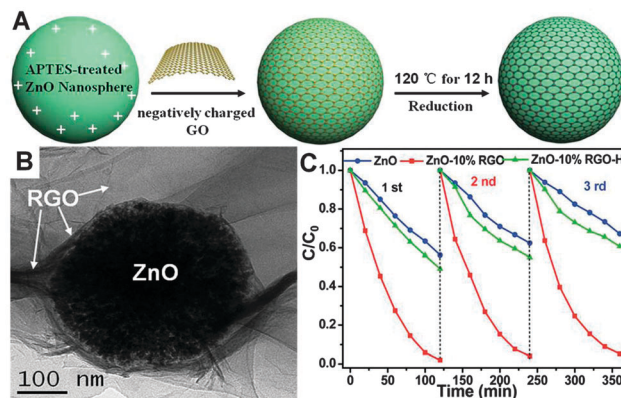


Fig. 7 (A) Schematic flowchart for electrostatic self-assembly of ZnO–RGO nanocomposites; (B) TEM image of ZnO–10% RGO; and (C) recycling photocatalytic degradation of Rhodamine B (RhB) over ZnO, ZnO–10% RGO and ZnO–10% RGO–H prepared by hard integration under UV light irradiation ( $\lambda = 350 \pm 15$  nm) at room temperature in the aqueous phase. Reprinted with permission from ref. 101. Copyright 2014 Royal Society of Chemistry.

controlling the morphology of GR–semiconductor composites in a uniform manner by pre-selection of semiconductors with desirable architectural morphology.<sup>100–104</sup> In addition, this synthesis method also enables the photoactivity comparison to be carried out in a framework in which morphology difference between bare semiconductors and semiconductors in GR–semiconductor composites is excluded,<sup>100–104</sup> whereas this cannot be strictly ruled out in the above case. Using this self-assembly method, Xu *et al.* have reported the synthesis of ZnO–RGO composites, which display uniform, well-controlled morphology, good interfacial contact and improved photoactivity as shown in Fig. 7B and C.<sup>101</sup> The intimate surface coating with GR even improves the anti-photocorrosion of semiconductor ZnO in the aqueous phase more effectively than ZnO–RGO–H composites with poor interfacial contact (Fig. 7C). The improved photoactivity and anti-photocorrosion of ZnO–RGO can be attributed to the following: (i) the intimate interfacial contact between ZnO and RGO is favorable to utilize the excellent electron conductivity of GR to transfer the photogenerated charge carriers and lengthen the lifetime of charge carriers more effectively; (ii) the package of ZnO with RGO could amplify the role of RGO for passivating the ZnO surface and working as a protective shield to avoid the photocorrosion of ZnO, whereas this effect cannot be obtained over ZnO–RGO–H due to poor interfacial interaction; and (iii) the introduction of RGO could adsorb RhB molecules through  $\pi$ – $\pi$  conjugation between the dye and aromatic regions of RGO, and the RhB molecules will directly react with photoinduced holes which would compete with the

photocorrosion processes, resulting in the improvement of anti-photocorrosion.

Apart from ZnO, some other GR–semiconductor nanocomposites have also been reported by this surface charge modified electrostatic self-assembly approach. For example, Park *et al.* have prepared TiO<sub>2</sub> nanoparticles (NPs) coated with GR by the self-assembly of positively charged TiO<sub>2</sub> with negatively charged GO nanosheets followed by a reduction of GO to GR (Fig. 8A).<sup>100</sup> The GR–TiO<sub>2</sub> NPs exhibit improved visible light photoactivity toward degradation of methylene blue (MB), as shown in Fig. 8B. This can be attributed to the tight coating of TiO<sub>2</sub> with GR, which narrows the bandgap of the hybrid material, enhances the absorption of visible light and allows more efficient transfer of photogenerated electrons from excited MB to TiO<sub>2</sub> NPs through graphene nanosheets.<sup>100</sup>

Analogously, Lu *et al.* have fabricated the BiVO<sub>4</sub>–RGO nanocomposites with efficient interfacial contact by self-assembly of amine-functionalized BiVO<sub>4</sub> powders with GO, followed by a one-step GO reduction and BiVO<sub>4</sub> crystallization *via* hydrothermal treatment.<sup>106</sup> The adequate interfacial interaction between BiVO<sub>4</sub> and RGO not only improves the photogenerated charge carrier separation efficiency, but also prevents the aggregation of BiVO<sub>4</sub> particles during the hydrothermal crystallization process (Fig. 8C and D). Consequently, the BiVO<sub>4</sub>–RGO nanocomposites exhibit high visible light photocatalytic efficiency for the degradation of model dye, and are significantly superior to bare crystalline BiVO<sub>4</sub> and BiVO<sub>4</sub>–RGO–U that is hydrothermally synthesized using the mixture of GO nanosheets and BiVO<sub>4</sub>

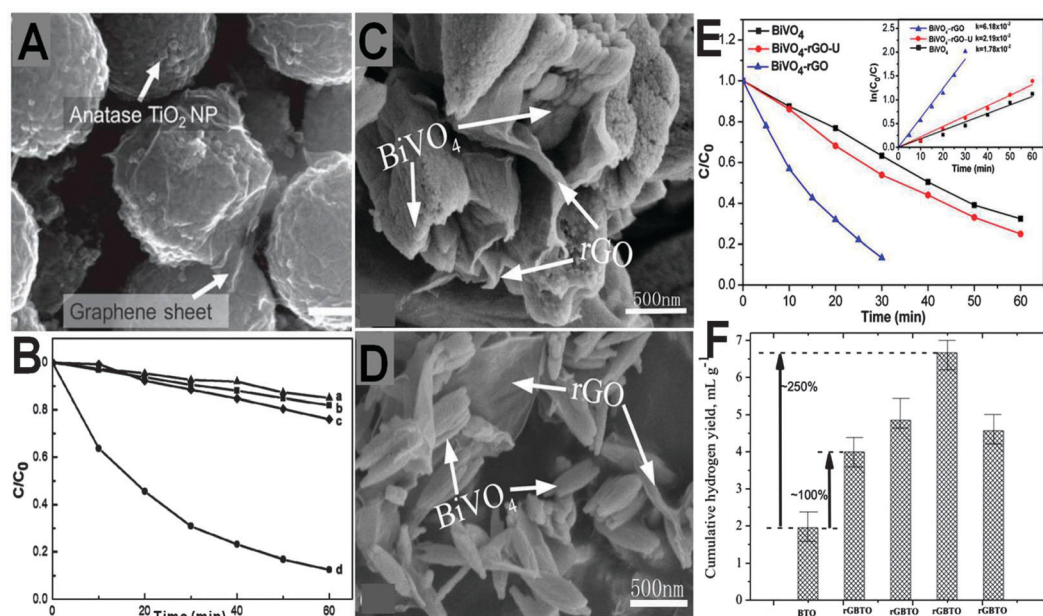


**Fig. 8** (A) SEM image of GR–TiO<sub>2</sub> NPs; (B) photodegradation of MB under visible light irradiation ( $\lambda > 420$  nm) by (a) P25, (b) bare anatase TiO<sub>2</sub> NPs, (c) GR–TiO<sub>2</sub> NPs (two-step hydrothermal), and (d) GR–TiO<sub>2</sub> NPs. Reprinted with permission from ref. 100. Copyright 2012, John Wiley & Sons, Inc. SEM images of (C) BiVO<sub>4</sub>–RGO–U and (D) BiVO<sub>4</sub>–RGO; (E) photodegradation of rhodamine B (RhB) under visible light ( $\lambda > 400$  nm) over the bare BiVO<sub>4</sub>, BiVO<sub>4</sub>–RGO–U, and BiVO<sub>4</sub>–RGO photocatalysts; and (F) the cumulative hydrogen yield obtained using the pristine BTO and the RGO–BTO composite catalysts with RGO content varied from 0.25 wt% to 6 wt%. The results presented in this bar graph are obtained in the presence of a water/methanol mixture with 250/50 (v/v) composition and UV–vis illumination continuously over a period of 130 minutes. Reprinted with permission from ref. 106 and 107. Copyright 2014, 2014, American Chemical Society.

powders without modification of surface charge (Fig. 8E). In addition, in a very recent study of Subramanian *et al.*, RGO–Bi<sub>2</sub>Ti<sub>2</sub>O<sub>7</sub> (BTO) nanocomposites were prepared *via* the same method.<sup>107</sup> Owing to the better interfacial contact between RGO and BTO through the self-assembly approach and the unique ability of the RGO to promote charge transport, the RGO–Bi<sub>2</sub>Ti<sub>2</sub>O<sub>7</sub> also displays improved photoactivity and sustainable photostability toward the photocatalytic H<sub>2</sub> evolution reaction (Fig. 8F). These literature reports demonstrate that to alleviate the rapid recombination of photoinduced electron–hole pairs in the excited states that significantly lower the efficiency of semiconductor photocatalysis,<sup>16,18</sup> strengthening the interfacial contact between GR and semiconductors to maximize the interfacial charge carrier transfer efficiency can be a promising strategy to improve the semiconductor photoactivity in a more effective way.

### 3.3 Systems materials engineering of graphene–semiconductor composite photocatalysts

The above strategies primarily rely on the better utilization of electronic conductivity of GR by either improving the electronic conductivity of GR or strengthening the interfacial contact between GR and semiconductors, thereby boosting the photoactivity for specific photoredox reactions.<sup>41,59,68,69,100</sup> Nevertheless, these strategies often focus on only investigating the isolated constituents instead of optimizing the entire system of GR–semiconductor composites.<sup>41,59,68,69,100</sup> Recently, the development of modern materials science has strongly suggested that investigating isolated components within a device or catalyst system is no longer sufficient to solve challenges involved in the development of an environmentally benign energy infrastructure.<sup>108,109</sup> To design an efficient artificial photosynthetic materials system, the integration of individual components into a complete and functioning system while simultaneously optimizing the resulting interfaces is needed.<sup>108,109</sup> As displayed in Fig. 9, the systems materials engineering triangle schematically illustrates the importance of system-level planning of the research effort starting from individual components and followed by interface optimization.<sup>109</sup>

These insightful perspectives enlighten us that the optimization of the overall photocatalytic performance for a specific GR–semiconductor composite system should be at the system level which particularly accentuates the study of interactions of individual components integrated in the entire composite system. In particular, in order to utilize the electronic conductivity of GR toward improving the separation and transfer of photogenerated charge carriers, it is highly crucial to optimize the interfacial composition of GR–semiconductor composites. In this regard, Xu *et al.* have recently proposed a conceptually new strategy to improve the photoactivity of GR–semiconductor CdS composites *via* the addition of a tiny amount of metal ions (M = Ca<sup>2+</sup>, Cr<sup>3+</sup>, Mn<sup>2+</sup>, Fe<sup>2+</sup>, Co<sup>2+</sup>, Ni<sup>2+</sup>, Cu<sup>2+</sup>, and Zn<sup>2+</sup>) into the interfacial layer to optimize the interfacial composition, while the intimate interfacial contact is maintained (Fig. 10A).<sup>110</sup> The roles of metal ions are two-fold. The first is to act as “generic interfacial mediator” to boost the lifetime and transfer efficiency of photogenerated charge carriers from CdS to the GR sheet. The CdS–(GR–M) composites exhibit significantly enhanced photoactivity compared to the optimal CdS–5%GR

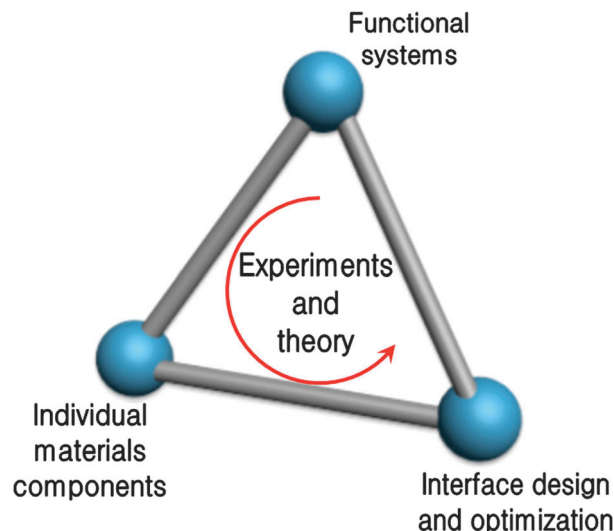


Fig. 9 Systems materials engineering triangle. Reprinted with permission from ref. 109. Copyright 2012 Nature Publishing Group.

(Fig. 10B and C). The second role is to partially counterbalance the negative light “shielding effect” of GR induced by the higher weight addition of GR. The optimal weight addition ratio of GR in CdS–(GR–M) is remarkably increased to 10% and even 30% in comparison with the optimal CdS–5%GR. In addition, among the optimal CdS–(GR–M) (M = Ca<sup>2+</sup>, Cr<sup>3+</sup>, Mn<sup>2+</sup>, Fe<sup>2+</sup>, Co<sup>2+</sup>, Ni<sup>2+</sup>, Cu<sup>2+</sup>, and Zn<sup>2+</sup>) nanocomposites, the modest difference in the photocatalytic activity of these samples could be primarily explained by the differences in the contents, microscopic distribution, and intrinsic electronic property of the metal ions as interfacial mediators between GR and semiconductor CdS,<sup>110</sup> which result in the different degrees in prolonging the lifetime and enhancing the transfer of charge carriers, and thus different photocatalytic performances.

Therefore, the strategy of using metal ions as interfacial mediators manifests the feasibility of promoting the photoactivity of a GR–semiconductor composite by optimizing the system from the angle of the systems materials engineering concept.<sup>110</sup> The significant issue of improving the photoactivity of GR–semiconductor composites is not just an issue of tighter connection or intimate interfacial contact between GR and semiconductors, but it is also the optimization of the atomic charge carrier transfer pathway across the interface.<sup>110</sup> However, in addition to interface optimization, the consideration of optimizing individual components, *i.e.*, GR and semiconductors, has not been performed yet, which can be further extended and developed, and this would significantly harmonize the entire GR–semiconductor composite system toward unprecedented photoactivity improvement.

## 4. Assembly of graphene–semiconductor composites with controllable film infrastructure

In most practical applications, the fixation of semiconductor photocatalysts on specific substrates to form films is required.<sup>111,112</sup>

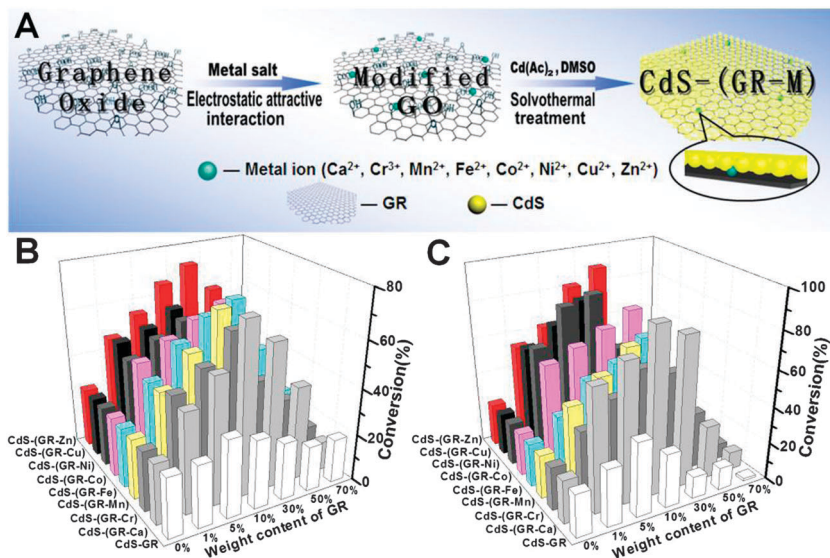


**Fig. 10** (A) Flowchart illustrating the fabrication of CdS-(GR-M) ( $M = \text{Ca}^{2+}$ ,  $\text{Cr}^{3+}$ ,  $\text{Mn}^{2+}$ ,  $\text{Fe}^{2+}$ ,  $\text{Co}^{2+}$ ,  $\text{Ni}^{2+}$ ,  $\text{Cu}^{2+}$ , and  $\text{Zn}^{2+}$ ) nanocomposites in which metal ions are introduced to the interfacial layer matrix between GR and semiconductor CdS; photocatalytic performance of blank CdS, CdS-GR, and CdS-(GR-M) ( $M = \text{Ca}^{2+}$ ,  $\text{Cr}^{3+}$ ,  $\text{Mn}^{2+}$ ,  $\text{Fe}^{2+}$ ,  $\text{Co}^{2+}$ ,  $\text{Ni}^{2+}$ ,  $\text{Cu}^{2+}$ , and  $\text{Zn}^{2+}$ ) nanocomposites with different weight addition ratios of GR for (B) photocatalytic selective oxidation of benzyl alcohol under visible light ( $\lambda > 420 \text{ nm}$ ) for 2 h and (C) selective reduction of 4-nitroaniline under visible light irradiation ( $\lambda > 420 \text{ nm}$ ) for 80 min. Reprinted with permission from ref. 110. Copyright 2014 American Chemical Society.

A fixed photocatalytic system allows for the continuous use of the photocatalysts for processing target reactions in gas and liquid phases while alleviating the drawback of post-process filtration coupled with powder catalyst recovery and regeneration.<sup>111,112</sup> Although various GR-semiconductor composites for extensive photoredox processes have been reported,<sup>1-13,15-123</sup> it is challenging to make uniform GR-semiconductor composite films with controllable film thickness and architecture, which are of paramount importance to meet the photocatalytic application requirements.<sup>113</sup>

Liu *et al.* have recently fabricated GR-semiconductor CdS quantum dot (QD) composite film photocatalysts using the layer-by-layer (LbL) self-assembly approach, known as a versatile bottom-up nanofabrication technique with simple benchmark operation (Fig. 11A).<sup>113</sup> The judicious integration of semiconductor CdS QDs with GR nanosheets (GNs) in an alternating manner shows that the GN films with thickness of several nanometers along with monodispersed deposition of semiconductor CdS in the nanometer regime on GNs have been achieved simultaneously. The architecture, photoelectrochemical and photocatalytic properties of GNs-CdS QD films can be tuned by simple control of deposition cycles. As shown in Fig. 11B and C, the loading density of CdS QDs on the surface of GNs varies substantially with the deposition cycles, indicating that the amount of CdS QDs during the LbL self-assembly process can be tuned by deposition cycles. Fig. 11D shows the transient photocurrent responses for CdS QDs, GNs, and (GNs-CdS QDs)<sub>n</sub> ( $n = 1, 5, 10, 15, 20$ ) multilayered films under visible light irradiation and under zero bias conditions. It is seen that the photocurrent of the GN-CdS QD multilayered films also changes with the number of deposition cycles and reaches a maximum at 15 cycles, which is caused by the competition of photon absorption between CdS QDs and GNs. In such a

hybrid film, the large and flat GNs not only perform as a support substrate for the immobilization of CdS QDs, but also serve as an electron mediator to separate and shuttle photo-generated electron-hole pairs. Consequently, the as-synthesized multilayered film composites show higher photoactivities toward selective reduction of nitroaromatic compounds under visible light than pure CdS QD film as exemplified in Fig. 11E.<sup>113</sup>

This work is a forward step to meet the application requirements of GR-semiconductor photocatalysts. However, it is worth noting that (i) the respective composition ratio in GN-CdS QD films is not optimized and (ii) the interfacial composition optimization has not been considered.<sup>113</sup> Therefore, the photoactivity for nitro reduction over GN-CdS QD films is much lower than that reported by Xu *et al.*<sup>110</sup> To envision that the generic interfacial mediator strategy (*e.g.*, introducing metal ions or other heteroatoms into the interfacial domain), proposed by Xu *et al.*,<sup>110</sup> may be rationally grafted with the controllable film architecture proposed by Liu *et al.*,<sup>113</sup> the highly efficient GR-semiconductor film photocatalyst with tunable photoelectronic properties would be wisely integrated in an optimal system level,<sup>109</sup> as depicted in Fig. 11F.

Additionally, other synthetic routes, *e.g.*, electrophoretic deposition,<sup>128,129</sup> Langmuir-Blodgett deposition,<sup>130,131</sup> vacuum filtration,<sup>132,133</sup> solution casting,<sup>134</sup> drop casting,<sup>135</sup> dip coating,<sup>136</sup> and spin coating,<sup>137</sup> have also been adopted to fabricate conductive GR films with large-area uniformity and high-quality. In particular, some of these methods have been reported to fabricate GR-semiconductor film photocatalysts with improved photoactivities (Table 1). Coupling with rational interfacial optimization and consideration of individual GR or semiconductors, it is conceivable to integrate the intrinsic outstanding properties of GR and semiconductors within the film structure,

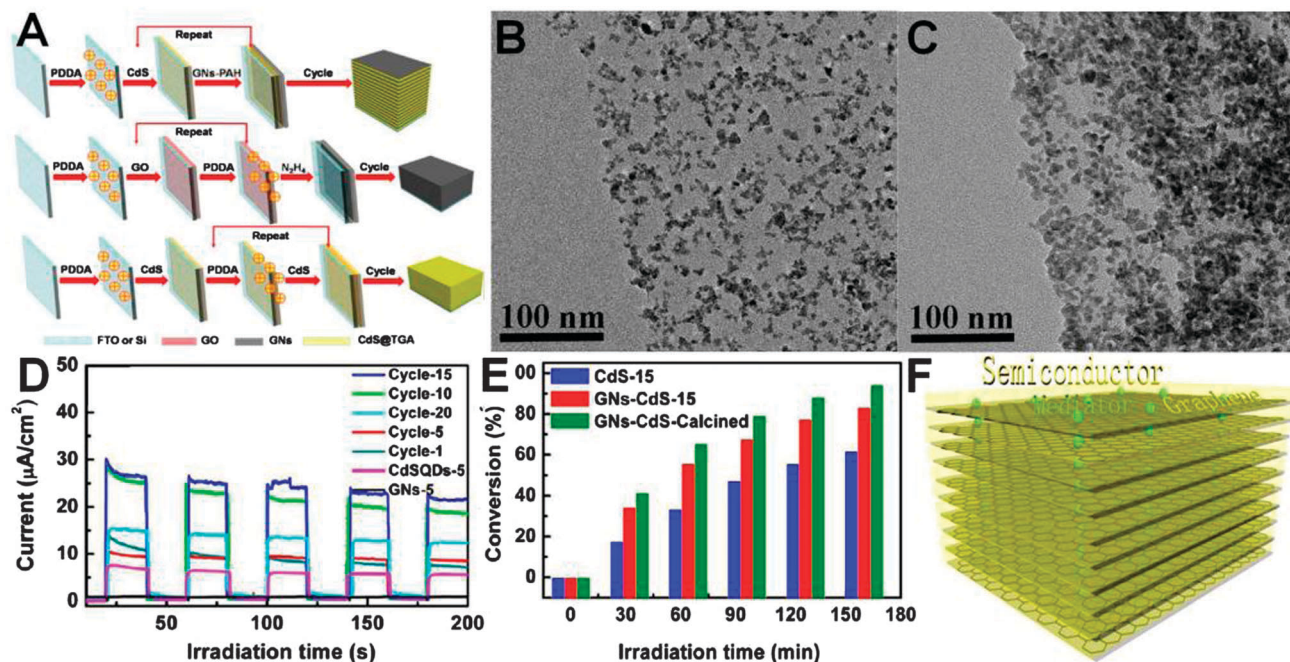


Fig. 11 (A) Schematic illustration for LbL bottom-up self-assembly of GN-CdS QDs, pure GNs, and pure CdS QD multilayered films; TEM images of GN-CdS QD composite film with (B) one and (C) five deposition cycles peeled off from FTO substrate; (D) transient photocurrent responses of CdS QDs and GN films with five deposition cycles, and (GNs-CdS QDs)<sub>n</sub> (*n* = 1, 5, 10, 15, 20) multilayered films; (E) photocatalytic performance of CdS QD film (15 cycles), as-assembled GN-CdS QD composite film (15 cycles), and calcined GN-CdS QD composite films (15 cycles) for selective reduction of 4-nitroaniline under visible light irradiation ( $\lambda > 420$  nm). Reprinted with permission from ref. 113. Copyright 2014 American Chemical Society. (F) Proposed fabrication of (GNs-M)-CdS QD films with metal ions or other heteroatoms as interfacial mediator.

Table 1 Some recent reports of graphene-based nanocomposite film toward target photocatalytic applications

Synthetic method	Composite photocatalyst	Light source	Photocatalytic applications	Photocatalytic activity enhancement	Ref.
Spin-coating	GR-TiO <sub>2</sub>	UV light, 40 W cylindrical black light bulb	Degradation of MB	2-fold of blank TiO <sub>2</sub>	114
	GO-TiO <sub>2</sub>	UV/vis light, 20 W UV and fluorescent lamps	Degradation of MB	UV light, 2.3-fold of blank TiO <sub>2</sub> Vis light, 2.2-fold of blank TiO <sub>2</sub>	115
	GR-TiO <sub>2</sub>	UV light, 250 W high-pressure mercury	Degradation of Reactive Brilliant Red dye X-3B	No reference photocatalyst	116
	GR-La <sub>1-x</sub> Sr <sub>x</sub> MnO <sub>3</sub>	UV-vis light, 300 W xenon lamp	Degradation of acid red 3GN	1.6-fold of P25 and 1.3-fold of LaMnO <sub>3</sub>	117
	GR-TiO <sub>2</sub>	UV light, 20 W black-light (UVA) lamps	Degradation of acid red MB	2.5-fold of blank TiO <sub>2</sub>	118
Dip-coating	GR/Fe <sup>3+</sup> -TiO <sub>2</sub>	UV/vis light	Degradation of and formaldehyde	UV light, 2.3-fold of blank TiO <sub>2</sub> Vis light, 2-fold of blank TiO <sub>2</sub>	119
Electrophoretic deposition	GR-TiO <sub>2</sub> nanotube array	Vis light, 35 W xenon lamp	Degradation of MB	1.6-fold of TiO <sub>2</sub> nanotube array	120
Electrostatic spray deposition	GR-ZnO	UV light (0.6 mW cm <sup>-2</sup> )	Degradation of MB	1.3-fold of blank ZnO	121
Drop-casting	GR-TiO <sub>2</sub>	UV light, mercury lamp	Degradation of RhB	1.7-fold of blank TiO <sub>2</sub>	122
	GR-TiO <sub>2</sub>	Solar light	Photoinactivation of <i>Escherichia coli</i> bacteria	7.5-fold of blank TiO <sub>2</sub>	123
	GR-WO <sub>3</sub>	Vis light, 110 mW cm <sup>-2</sup> mercury lamp	Photoinactivation of bacteriophage MS <sub>2</sub> viruses	5-fold of blank WO <sub>3</sub>	124
Vacuum filtration	GR-TiO <sub>2</sub>	UV light, 450 W Xe lamp	Degradation of 2,4-D	4-fold of blank TiO <sub>2</sub>	125
	GR/ <i>p</i> -THPP	Vis light, 500 W Xe lamp	Degradation of RhB and MB	RhB, 2-fold of blank <i>p</i> -THPP MB, 2.1-fold of blank <i>p</i> -THPP	126
Radio frequency (RF) magnetron sputtering	GR-TiO <sub>2</sub>	UV light, 100 W mercury lamp	Degradation of MO	1.2-fold of blank TiO <sub>2</sub>	127

Note: MB is methylene blue; RhB is rhodamine B; MO is methyl orange; 2,4-D is 2,4-dichlorophenoxyacetic acid; and *p*-THPP is porphyrin (*meso*-tetra(*p*-hydroxyphenyl)porphyrin).

and thus the efficient GR–semiconductor film photocatalyst with robust structural and functional infrastructure for practical applications would become available in the future.

## 5. Conclusions and future outlook

There is no doubt that graphene has an impressive set of properties and holds great potential in many fields, including the area of energy conversion and storage. Coupling graphene with semiconductor materials in a suitable manner provides us with promising opportunities to design the next-generation artificial photosynthesis systems with high performance. However, after passing the zenith of praise on GR, it should be increasingly rational to be conscious of the high importance of focusing on how to sufficiently unleash the fascinating properties of GR, particularly for the electronic conductivity, in GR–semiconductor composites, aiming to improve their photocatalytic performance more effectively. To further the research in this area and realize the photocatalytic applications, the materials processing effort should shift to designing GR–semiconductor composites in a systems materials engineering way.

To be specific, firstly, the individual components (*i.e.*, GR and semiconductors) in the composites should be optimized, including tuning the size, shape, morphology and electronic conductivity of individual GR and semiconductors, all of which have proven to be important factors that would integratively influence the photocatalytic performance of the resulting GR–semiconductor composites. For example, the fabrication of the GR–semiconductor with special dimensionality structures (*e.g.* 1D semiconductor–2D graphene, 2D-semiconductor–2D graphene) has proven to be a promising way to further enhance the photoactivity of graphene–semiconductor composites. Secondly, the interfacial contact between GR and semiconductors should be rationally strengthened. As discussed above, since the photogenerated charge carrier transfer predominantly occurs across the interfacial domain in the GR–semiconductor composite systems, maximizing the interfacial contact between GR and the photoactive semiconductor would be an effective strategy for better harnessing the electronic conductivity of GR, thereby enhancing the separation and transfer of photogenerated charge carriers and thus improving the overall photocatalytic efficiency of GR–semiconductor nanocomposites. Thirdly, the atomic charge carrier transfer pathway across the interface between the semiconductor and GR should be optimized. Given this issue, introducing a small amount of heteroatoms, *e.g.*, metal ions or metal particles, into the interfacial layer matrix between GR and semiconductors would further contribute to spatially facilitating the microscopic charge carrier transfer pathway. In addition, interface band bending calculations in theory should be adopted, which would aid us to fundamentally and deeply understand the photogenerated charge carrier transfer pathway, efficiency across the interfacial domain. Thus, a joint effort between experiment and theory leads to the better targeted design of GR–semiconductor nanocomposites with improved performance.

In fact, the issue of the overall photocatalytic performance of GR–semiconductor composites can never be attributed to a single factor (*e.g.*, the “panacea” attribution of photoactivity enhancement to the excellent electronic conductivity of GR), but instead a collective, harmonious integration of the individual components, interface composition, and material’s structure and morphology at the nanoscale. Independent of perfect or defective GR, each type of GR has its advantages and limits; different applications require different grades of GR. For fabricating GR–semiconductor composite photocatalysts with high performance, the system-level consideration of individual GR, semiconductors and interface optimization is necessary.

With a rational and historical view of the revolutionary path from a fundamental understanding to practical applications of any material, the construction of the next-generation of photocatalytic systems based on GR–semiconductor composites would take a much longer time and requires sustained effort and interest from the researchers. But, one thing is certain that, only with the principle of designing and understanding GR–semiconductor composites from a system-level consideration, we could get better at imparting the power of GR with unique and transformative properties into the composite system, thereby bringing closer the widespread practical implementation of this unique composite material in artificial photocatalysis.

## Acknowledgements

The support from the National Natural Science Foundation of China (NSFC) (21173045, 20903023), the Award Program for Minjiang Scholar Professorship, the Natural Science Foundation (NSF) of Fujian Province for Distinguished Young Investigator Grant (2012J06003), and Program for Returned High-Level Overseas Chinese Scholars of Fujian Province is gratefully acknowledged.

## Notes and references

- 1 X. Chen, C. Li, M. Gratzel, R. Kostecki and S. S. Mao, *Chem. Soc. Rev.*, 2012, **41**, 7909–7937.
- 2 C. Liu, N. P. Dasgupta and P. Yang, *Chem. Mater.*, 2013, **26**, 415–422.
- 3 D. Gust, T. A. Moore and A. L. Moore, *Acc. Chem. Res.*, 2009, **42**, 1890–1898.
- 4 R. K. Yadav, J.-O. Baeg, G. H. Oh, N.-J. Park, K.-j. Kong, J. Kim, D. W. Hwang and S. K. Biswas, *J. Am. Chem. Soc.*, 2012, **134**, 11455–11461.
- 5 J. C. Colmenares and R. Luque, *Chem. Soc. Rev.*, 2014, **43**, 765–778.
- 6 S. Choudhury, J.-O. Baeg, N.-J. Park and R. K. Yadav, *Green Chem.*, 2014, **16**, 4389–4400.
- 7 T. Zhang and W. Lin, *Chem. Soc. Rev.*, 2014, **43**, 5982–5993.
- 8 T. Faunce, S. Styring, M. R. Wasielewski, G. W. Brudvig, A. W. Rutherford, J. Messinger, A. F. Lee, C. L. Hill, H. deGroot, M. Fontecave, D. R. MacFarlane, B. Hankamer, D. G. Nocera, D. M. Tiede, H. Dau, W. Hillier, L. Wang and R. Amal, *Energy Environ. Sci.*, 2013, **6**, 1074–1076.

- 9 A. Fujishima and K. Honda, *Nature*, 1972, **238**, 37–38.
- 10 L. Jing, W. Zhou, G. Tian and H. Fu, *Chem. Soc. Rev.*, 2013, **42**, 9509–9549.
- 11 J. Ran, J. Zhang, J. Yu, M. Jaroniec and S. Z. Qiao, *Chem. Soc. Rev.*, 2014, DOI: 10.1039/c3cs60425j.
- 12 X. Lang, X. Chen and J. Zhao, *Chem. Soc. Rev.*, 2014, **43**, 473–486.
- 13 K. S. Novoselov, A. K. Geim, S. V. Morozov, D. Jiang, Y. Zhang, S. V. Dubonos, I. V. Grigorieva and A. A. Firsov, *Science*, 2004, **306**, 666–669.
- 14 Y. Zhang, Z.-R. Tang, X. Fu and Y.-J. Xu, *ACS Nano*, 2010, **4**, 7303–7314.
- 15 N. Zhang, Y. Zhang and Y.-J. Xu, *Nanoscale*, 2012, **4**, 5792–5813.
- 16 Q. Xiang, J. Yu and M. Jaroniec, *Chem. Soc. Rev.*, 2012, **41**, 782–796.
- 17 L. Han, P. Wang and S. Dong, *Nanoscale*, 2012, **4**, 5814–5825.
- 18 M.-Q. Yang and Y.-J. Xu, *Phys. Chem. Chem. Phys.*, 2013, **15**, 19102–19118.
- 19 P. V. Kamat, *J. Phys. Chem. Lett.*, 2011, **2**, 242–251.
- 20 Y. Zhang, N. Zhang, Z.-R. Tang and Y.-J. Xu, *ACS Nano*, 2012, **6**, 9777–9789.
- 21 I. V. Lightcap and P. V. Kamat, *Acc. Chem. Res.*, 2013, **46**, 2235–2243.
- 22 X. An and J. C. Yu, *RSC Adv.*, 2011, **1**, 1426–1434.
- 23 H. Zhang, X. Lv, Y. Li, Y. Wang and J. Li, *ACS Nano*, 2010, **4**, 380–386.
- 24 G. Xie, K. Zhang, B. Guo, Q. Liu, L. Fang and J. R. Gong, *Adv. Mater.*, 2013, **25**, 3820–3839.
- 25 Q. Xiang and J. Yu, *J. Phys. Chem. Lett.*, 2013, **4**, 753–759.
- 26 W. Tu, Y. Zhou and Z. Zou, *Adv. Funct. Mater.*, 2013, **23**, 4996–5008.
- 27 W. Tu, Y. Zhou, Q. Liu, Z. Tian, J. Gao, X. Chen, H. Zhang, J. Liu and Z. Zou, *Adv. Funct. Mater.*, 2012, **22**, 1215–1221.
- 28 W. Tu, Y. Zhou, Q. Liu, S. Yan, S. Bao, X. Wang, M. Xiao and Z. Zou, *Adv. Funct. Mater.*, 2013, **23**, 1743–1749.
- 29 N. Zhang, Y. Zhang, M.-Q. Yang and Y.-J. Xu, *Curr. Org. Chem.*, 2013, **17**, 2503–2515.
- 30 M.-Q. Yang, Y. Zhang, N. Zhang, Z.-R. Tang and Y.-J. Xu, *Sci. Rep.*, 2013, **3**, 3314–3320.
- 31 Y. Sun, Q. Wu and G. Shi, *Energy Environ. Sci.*, 2011, **4**, 1113–1132.
- 32 J. Kim, L. J. Cote, F. Kim, W. Yuan, K. R. Shull and J. Huang, *J. Am. Chem. Soc.*, 2010, **132**, 8180–8186.
- 33 J. Luo, L. J. Cote, V. C. Tung, A. T. L. Tan, P. E. Goins, J. Wu and J. Huang, *J. Am. Chem. Soc.*, 2010, **132**, 17667–17669.
- 34 J. Kim, L. J. Cote and J. Huang, *Acc. Chem. Res.*, 2012, **45**, 1356–1364.
- 35 D. R. Dreyer, S. Park, C. W. Bielawski and R. S. Ruoff, *Chem. Soc. Rev.*, 2010, **39**, 228–240.
- 36 K. P. Loh, Q. Bao, G. Eda and M. Chhowalla, *Nat. Chem.*, 2010, **2**, 1015–1024.
- 37 Y. Zhang, N. Zhang, Z.-R. Tang and Y.-J. Xu, *J. Phys. Chem. C*, 2014, **118**, 5299–5308.
- 38 M.-Q. Yang, X. Pan, N. Zhang and Y.-J. Xu, *CrystEngComm*, 2013, **15**, 6819–6828.
- 39 X. Chen, G. Wu, J. Chen, X. Chen, Z. Xie and X. Wang, *J. Am. Chem. Soc.*, 2011, **133**, 3693–3695.
- 40 M.-Q. Yang and Y.-J. Xu, *J. Phys. Chem. C*, 2013, **117**, 21724–21734.
- 41 B. Qiu, M. Xing and J. Zhang, *J. Am. Chem. Soc.*, 2014, **136**, 5852–5855.
- 42 N. Zhang, Y. Zhang, X. Pan, X. Fu, S. Liu and Y.-J. Xu, *J. Phys. Chem. C*, 2011, **115**, 23501–23511.
- 43 G. Williams, B. Seger and P. V. Kamat, *ACS Nano*, 2008, **2**, 1487–1491.
- 44 X. Liu, L. Pan, T. Lv, G. Zhu, Z. Sun and C. Sun, *Chem. Commun.*, 2011, **47**, 11984–11986.
- 45 P. Chen, T.-Y. Xiao, H.-H. Li, J.-J. Yang, Z. Wang, H.-B. Yao and S.-H. Yu, *ACS Nano*, 2011, **6**, 712–719.
- 46 M. Zhu, P. Chen and M. Liu, *ACS Nano*, 2011, **5**, 4529–4536.
- 47 A. K. Geim and K. S. Novoselov, *Nat. Mater.*, 2007, **6**, 183–191.
- 48 A. K. Geim, *Science*, 2009, **324**, 1530–1534.
- 49 Y. Zhang, T.-T. Tang, C. Girit, Z. Hao, M. C. Martin, A. Zettl, M. F. Crommie, Y. R. Shen and F. Wang, *Nature*, 2009, **459**, 820–823.
- 50 M. F. Craciun, S. Russo, M. Yamamoto, J. B. Oostinga, A. F. Morpurgo and S. Tarucha, *Nat. Nanotechnol.*, 2009, **4**, 383–388.
- 51 W. S. Hummers and R. E. Offeman, *J. Am. Chem. Soc.*, 1958, **80**, 1339.
- 52 J. Zhang, Z. Xiong and X. S. Zhao, *J. Mater. Chem.*, 2011, **21**, 3634–3640.
- 53 J. Zhou, G. Tian, Y. Chen, X. Meng, Y. Shi, X. Cao, K. Pan and H. Fu, *Chem. Commun.*, 2013, **49**, 2237–2239.
- 54 H. Zhang, X. Fan, X. Quan, S. Chen and H. Yu, *Environ. Sci. Technol.*, 2011, **45**, 5731–5736.
- 55 F. Banhart, J. Kotakoski and A. V. Krasheninnikov, *ACS Nano*, 2010, **5**, 26–41.
- 56 C. Gomez-Navarro, J. C. Meyer, R. S. Sundaram, A. Chuvilin, S. Kurasch, M. Burghard, K. Kern and U. Kaiser, *Nano Lett.*, 2010, **10**, 1144–1148.
- 57 P. V. Kamat, *J. Phys. Chem. Lett.*, 2009, **1**, 520–527.
- 58 S. Bai and X. Shen, *RSC Adv.*, 2012, **2**, 64–98.
- 59 Y. Zhang, Z.-R. Tang, X. Fu and Y.-J. Xu, *ACS Nano*, 2011, **5**, 7426–7435.
- 60 Q. Xiang, J. Yu and M. Jaroniec, *J. Am. Chem. Soc.*, 2012, **134**, 6575–6578.
- 61 J. Luo, J. Kim and J. Huang, *Acc. Chem. Res.*, 2013, **46**, 2225–2234.
- 62 Editorials, *Nature*, 2011, **473**, 419.
- 63 R. V. Noorden, *Nature*, 2011, **469**, 14–16.
- 64 Y. Hernandez, V. Nicolosi, M. Lotya, F. M. Blighe, Z. Sun, S. De, I. T. McGovern, B. Holland, M. Byrne, Y. K. Gun'Ko, J. J. Boland, P. Niraj, G. Duesberg, S. Krishnamurthy, R. Goodhue, J. Hutchison, V. Scardaci, A. C. Ferrari and J. N. Coleman, *Nat. Nanotechnol.*, 2008, **3**, 563–568.
- 65 J. N. Coleman, *Acc. Chem. Res.*, 2012, **46**, 14–22.
- 66 J. N. Coleman, *Adv. Funct. Mater.*, 2009, **19**, 3680–3695.
- 67 M. Lotya, Y. Hernandez, P. J. King, R. J. Smith, V. Nicolosi, L. S. Karlsson, F. M. Blighe, S. De, Z. Wang, I. T. McGovern,

- G. S. Duesberg and J. N. Coleman, *J. Am. Chem. Soc.*, 2009, **131**, 3611–3620.
- 68 Y. T. Liang, B. K. Vijayan, K. A. Gray and M. C. Hersam, *Nano Lett.*, 2011, **11**, 2865–2870.
- 69 Y. Zhang, N. Zhang, Z.-R. Tang and Y.-J. Xu, *Phys. Chem. Chem. Phys.*, 2012, **14**, 9167–9175.
- 70 X. Guangyu, Z. Yuegang, D. Xiangfeng, A. A. Balandin and K. L. Wang, *Proc. IEEE*, 2013, **101**, 1670–1688.
- 71 M. Jahan, Q. Bao, J.-X. Yang and K. P. Loh, *J. Am. Chem. Soc.*, 2010, **132**, 14487–14495.
- 72 N. Zhang, Y. Zhang, M.-Q. Yang, Z.-R. Tang and Y.-J. Xu, *J. Catal.*, 2013, **299**, 210–221.
- 73 L. Yuan, M.-Q. Yang and Y.-J. Xu, *J. Mater. Chem. A*, 2014, **2**, 14401–14412.
- 74 P. M. Sudeep, T. N. Narayanan, A. Ganesan, M. M. Shaijumon, H. Yang, S. Ozden, P. K. Patra, M. Pasquali, R. Vajtai, S. Ganguli, A. K. Roy, M. R. Anantharaman and P. M. Ajayan, *ACS Nano*, 2013, **7**, 7034–7040.
- 75 H. Yin, S. Zhao, J. Wan, H. Tang, L. Chang, L. He, H. Zhao, Y. Gao and Z. Tang, *Adv. Mater.*, 2013, **25**, 6270–6276.
- 76 Z. Chen, W. Ren, L. Gao, B. Liu, S. Pei and H.-M. Cheng, *Nat. Mater.*, 2011, **10**, 424–428.
- 77 S. Chen, J. Duan, M. Jaroniec and S. Z. Qiao, *Angew. Chem., Int. Ed.*, 2013, **52**, 13567–13570.
- 78 Z. Niu, J. Chen, H. H. Hng, J. Ma and X. Chen, *Adv. Mater.*, 2012, **24**, 4144–4150.
- 79 Y. Xu, K. Sheng, C. Li and G. Shi, *ACS Nano*, 2010, **4**, 4324–4330.
- 80 H. D. Pham, V. H. Pham, T. V. Cuong, T.-D. Nguyen-Phan, J. S. Chung, E. W. Shin and S. Kim, *Chem. Commun.*, 2011, **47**, 9672–9674.
- 81 W. Chen, S. Li, C. Chen and L. Yan, *Adv. Mater.*, 2011, **23**, 5679–5683.
- 82 H. Sun, L. Cao and L. Lu, *Energy Environ. Sci.*, 2012, **5**, 6206–6213.
- 83 L. Estevez, A. Kelarakis, Q. Gong, E. H. Da'as and E. P. Giannelis, *J. Am. Chem. Soc.*, 2011, **133**, 6122–6125.
- 84 J. L. Vickery, A. J. Patil and S. Mann, *Adv. Mater.*, 2009, **21**, 2180–2184.
- 85 B. G. Choi, M. Yang, W. H. Hong, J. W. Choi and Y. S. Huh, *ACS Nano*, 2012, **6**, 4020–4028.
- 86 J. W. Burrell, S. Gadipelli, J. Ford, J. M. Simmons, W. Zhou and T. Yildirim, *Angew. Chem., Int. Ed.*, 2010, **49**, 8902–8904.
- 87 G. Srinivas, J. W. Burrell, J. Ford and T. Yildirim, *J. Mater. Chem.*, 2011, **21**, 11323–11329.
- 88 M. A. Worsley, P. J. Pauzauskie, T. Y. Olson, J. Biener, J. H. Satcher and T. F. Baumann, *J. Am. Chem. Soc.*, 2010, **132**, 14067–14069.
- 89 S. Watcharotone, D. A. Dikin, S. Stankovich, R. Piner, I. Jung, G. H. B. Dommett, G. Evmenenko, S.-E. Wu, S.-F. Chen, C.-P. Liu, S. T. Nguyen and R. S. Ruoff, *Nano Lett.*, 2007, **7**, 1888–1892.
- 90 M. A. Worsley, T. Y. Olson, J. R. I. Lee, T. M. Willey, M. H. Nielsen, S. K. Roberts, P. J. Pauzauskie, J. Biener, J. H. Satcher and T. F. Baumann, *J. Phys. Chem. Lett.*, 2011, **2**, 921–925.
- 91 M. F. El-Kady, V. Strong, S. Dubin and R. B. Kaner, *Science*, 2012, **335**, 1326–1330.
- 92 V. Strong, S. Dubin, M. F. El-Kady, A. Lech, Y. Wang, B. H. Weiller and R. B. Kaner, *ACS Nano*, 2012, **6**, 1395–1403.
- 93 C. Li and G. Shi, *Nanoscale*, 2012, **4**, 5549–5563.
- 94 S. Nardecchia, D. Carriazo, M. L. Ferrer, M. C. Gutierrez and F. del Monte, *Chem. Soc. Rev.*, 2013, **42**, 794–830.
- 95 A. Iwase, Y. H. Ng, Y. Ishiguro, A. Kudo and R. Amal, *J. Am. Chem. Soc.*, 2011, **133**, 11054–11057.
- 96 N. Zhang, M.-Q. Yang, Z.-R. Tang and Y.-J. Xu, *J. Catal.*, 2013, **303**, 60–69.
- 97 S. Deng, V. Tjoa, H. M. Fan, H. R. Tan, D. C. Sayle, M. Olivo, S. Mhaisalkar, J. Wei and C. H. Sow, *J. Am. Chem. Soc.*, 2012, **134**, 4905–4917.
- 98 Q. Li, B. Guo, J. Yu, J. Ran, B. Zhang, H. Yan and J. R. Gong, *J. Am. Chem. Soc.*, 2011, **133**, 10878–10884.
- 99 X. Pan, M.-Q. Yang and Y.-J. Xu, *Phys. Chem. Chem. Phys.*, 2014, **16**, 5589–5599.
- 100 J. S. Lee, K. H. You and C. B. Park, *Adv. Mater.*, 2012, **24**, 1084–1088.
- 101 B. Weng, M.-Q. Yang, N. Zhang and Y.-J. Xu, *J. Mater. Chem. A*, 2014, **2**, 9380–9389.
- 102 Z. Chen, S. Liu, M.-Q. Yang and Y.-J. Xu, *ACS Appl. Mater. Interfaces*, 2013, **5**, 4309–4319.
- 103 M.-Q. Yang, B. Weng and Y.-J. Xu, *Langmuir*, 2013, **29**, 10549–10558.
- 104 S. Liu, Z. Chen, N. Zhang, Z.-R. Tang and Y.-J. Xu, *J. Phys. Chem. C*, 2013, **117**, 8251–8261.
- 105 L. Yuan, M.-Q. Yang and Y.-J. Xu, *Nanoscale*, 2014, **6**, 6335–6345.
- 106 Y. Wang, W. Wang, H. Mao, Y. Lu, J. Lu, J. Huang, Z. Ye and B. Lu, *ACS Appl. Mater. Interfaces*, 2014, **6**, 12698–12706.
- 107 S. Gupta and V. R. Subramanian, *ACS Appl. Mater. Interfaces*, 2014, DOI: 10.1021/am503396r.
- 108 H. Kitano, *Science*, 2002, **295**, 1662–1664.
- 109 P. Yang and J.-M. Tarascon, *Nat. Mater.*, 2012, **11**, 560–563.
- 110 N. Zhang, M.-Q. Yang, Z.-R. Tang and Y.-J. Xu, *ACS Nano*, 2014, **8**, 623–633.
- 111 N. Zhang, R. Ciriminna, M. Pagliaro and Y.-J. Xu, *Chem. Soc. Rev.*, 2014, **43**, 5276–5287.
- 112 M. R. Hoffmann, S. T. Martin, W. Choi and D. W. Bahnemann, *Chem. Rev.*, 1995, **95**, 69–96.
- 113 F.-X. Xiao, J. Miao and B. Liu, *J. Am. Chem. Soc.*, 2014, **136**, 1559–1569.
- 114 S. Anandan, T. Narasinga Rao, M. Sathish, D. Rangappa, I. Honma and M. Miyauchi, *ACS Appl. Mater. Interfaces*, 2012, **5**, 207–212.
- 115 D.-H. Yoo, T. V. Cuong, V. H. Pham, J. S. Chung, N. T. Khoa, E. J. Kim and S. H. Hahn, *Curr. Appl. Phys.*, 2011, **11**, 805–808.
- 116 P. Wang, Y. Ao, C. Wang, J. Hou and J. Qian, *J. Hazard. Mater.*, 2012, **223–224**, 79–83.
- 117 J. Hu, J. Ma, L. Wang and H. Huang, *Mater. Sci. Eng., B*, 2014, **180**, 46–53.
- 118 N. T. Khoa, M. W. Pyun, D.-H. Yoo, S. W. Kim, J.-Y. Leem, E. J. Kim and S. H. Hahn, *Thin Solid Films*, 2012, **520**, 5417–5420.
- 119 W. Low and V. Boonamnuayvitaya, *J. Environ. Manage.*, 2013, **127**, 142–149.

- 120 X. Cheng, H. Liu, Q. Chen, J. Li and P. Wang, *Carbon*, 2014, **66**, 450–458.
- 121 B. N. Joshi, H. Yoon, S.-H. Na, J.-Y. Choi and S. S. Yoon, *Ceram. Int.*, 2014, **40**, 3647–3654.
- 122 D. Wang, X. Li, J. Chen and X. Tao, *Chem. Eng. J.*, 2012, **198–199**, 547–554.
- 123 O. Akhavan and E. Ghaderi, *J. Phys. Chem. C*, 2009, **113**, 20214–20220.
- 124 O. Akhavan, M. Choobtashani and E. Ghaderi, *J. Phys. Chem. C*, 2012, **116**, 9653–9659.
- 125 Y. H. Ng, I. V. Lightcap, K. Goodwin, M. Matsumura and P. V. Kamat, *J. Phys. Chem. Lett.*, 2010, **1**, 2222–2227.
- 126 Y. Chen, Z.-H. Huang, M. Yue and F. Kang, *Nanoscale*, 2014, **6**, 978–985.
- 127 X. Liu, R. Cong, L. Cao, S. Liu and H. Cui, *New J. Chem.*, 2014, **38**, 2362–2367.
- 128 Z.-S. Wu, S. Pei, W. Ren, D. Tang, L. Gao, B. Liu, F. Li, C. Liu and H.-M. Cheng, *Adv. Mater.*, 2009, **21**, 1756–1760.
- 129 V. Lee, L. Whittaker, C. Jaye, K. M. Baroudi, D. A. Fischer and S. Banerjee, *Chem. Mater.*, 2009, **21**, 3905–3916.
- 130 L. J. Cote, F. Kim and J. Huang, *J. Am. Chem. Soc.*, 2008, **131**, 1043–1049.
- 131 X. Li, G. Zhang, X. Bai, X. Sun, X. Wang, E. Wang and H. Dai, *Nat. Nanotechnol.*, 2008, **3**, 538–542.
- 132 Y. Xu, H. Bai, G. Lu, C. Li and G. Shi, *J. Am. Chem. Soc.*, 2008, **130**, 5856–5857.
- 133 D. Li, M. B. Muller, S. Gilje, R. B. Kaner and G. G. Wallace, *Nat. Nanotechnol.*, 2008, **3**, 101–105.
- 134 S.-Y. Bae, I.-Y. Jeon, J. Yang, N. Park, H. S. Shin, S. Park, R. S. Ruoff, L. Dai and J.-B. Baek, *ACS Nano*, 2011, **5**, 4974–4980.
- 135 S. Gilje, S. Han, M. Wang, K. L. Wang and R. B. Kaner, *Nano Lett.*, 2007, **7**, 3394–3398.
- 136 X. Wang, L. Zhi and K. Mullen, *Nano Lett.*, 2007, **8**, 323–327.
- 137 H. A. Becerril, J. Mao, Z. Liu, R. M. Stoltenberg, Z. Bao and Y. Chen, *ACS Nano*, 2008, **2**, 463–470.